Journal of Marine Science and Application (2019) 18:417–432
https://doi.org/10.1007/s11804-019-00107-4

RESEARCH ARTICLE

Effect of Porosity on Oblique Wave Diffraction by Two Unequal Vertical Porous Barriers

Anjan Sasmal[1] · Sandip Paul[2] · Soumen De[1]

Received: 21 June 2018 / Accepted: 27 February 2019 / Published online: 17 October 2019

Abstract
The diffraction of obliquely incident wave by two unequal barriers with different porosity in infinitely deep water is investigated by using two-dimensional linearized potential theory. Reflection and transmission coefficients are computed numerically using appropriate Galerkin approximations for two partially immersed and two submerged barriers. The amount of energy dissipation due to the permeable barriers is derived using Green's integral theorem. The coefficient of wave force is determined using the linear Bernoulli equation of dynamic pressure jump on the porous barriers. The numerical results of hydrodynamics quantities are illustrated graphically.

Keywords Water wave scattering · Galerkin approximation · Porosity · Two unequal barriers · Reflection and transmission coefficients

1 Introduction

For the past several years, considerable interest has been focused on the problem of hydrodynamics analysis of breakwater due to its direct impact on coastal engineering. Vertical thin structures are widely used as breakwaters to protect harbors, inlets, and beaches from wave attack, due to their merits of simple structure and low engineering cost. Porous structures are more suitable for breakwater as dissipating seawalls to attenuate the wave energy in harbors. This finding justifies the interest in investigating these types of problems to examine the feasibility of using porous barriers as breakwater.

Studies on the diffraction of water wave problems by suitable arrangement of thin vertical barriers in deep water or finite depth water have been conducted by a number of researchers in recent years, in the literature within the framework of linearized theory of water wave. Ursell (1947) used an integral equation formulation of the problem to study the reflection coefficient that employs one-term Galerkin approximation for a single-surface piercing barrier in deep water. Several aspects of wave interaction with two thin vertical barriers were analyzed by Levine and Rodemich (1969), Jarvis (1971), Evans and Morris (1972), Newman (1974), McIver (1985), Isaacson et al. (1999), Das et al. (1997), Porter and Evans (1995), De et al. (2010), Kanoria and Mandal (1996), and Banerjea et al. (1996). Recently, the problem of obliquely incident water wave scattering by two unequal barriers was investigated by Roy et al. (2016) by applying the single-term Galerkin approximation.

None of the documented results account for the effect of porosity. However, many researchers have investigated the solutions for reflection and transmission coefficients for a certain type of porous barrier. The analytical solution of wave interaction through permeable breakwater was developed by Sollitt and Cross (1972). Macaskill (1979) obtained the solution of normally incident wave scattering involving a permeable thin barrier in water of infinite depth. Chwang (1983)

Article Highlights
- The problem of water wave scattering by two unequal partially immersed and submerged porous barriers in infinitely deep water is investigated.
- Using the Havelock expansion for the water wave potential, the problem is transformed into two integral equations, which are then approximated by employing single-term Galerkin approximation method.
- The reflection coefficient is depicted against the wave number in a number of figures.
- In the presence of porosity, the length and distance between barriers play an important role in the scattering behavior of the surface waves.

✉ Soumen De
soumenisi@gmail.com

[1] Department of Applied Mathematics, University of Calcutta, 700009, Kolkata, India

[2] Department of Mathematics, Dr. B.C.Roy Engineering College, 713206, Durgapur, India

developed a porous wavemaker theory in water of finite depth. Yu (1995) applied an approximate method to solve the problem of diffraction of surface water waves by a semi-infinite porous breakwater employing a boundary condition based on the formulation of Sollitt and Cross (1972). Isaacson et al. (1998) found the analytical solution for normally incident wave interaction with a partially immersed porous barrier. Lee and Chwang (2000) developed wave scattering and radiation by vertical thin porous barriers with four different structures based on the eigenfunction expansion and least square method. They found that the reflection coefficients and wave force of a porous barrier are smaller than those of the solid barrier, due to energy dissipation. Li et al. (2015) developed an accurate solution to water wave scattering by vertical thin porous barriers using multi-term Galerkin approximation. Manam and Sivanesan (2016) obtained the solution for deep water wave motion using an analytic approach over a surface piercing or a bottom-standing porous barrier. Bhattacharjee and Guedes Soares (2011) derived an analytical solution for the problem of water wave scattering by a vertical porous membrane barrier for a coastal structure near a wall by using eigenfunction expansion method and the corresponding orthogonal mode-coupling relation. Karmakar and Guedes Soares (2014) investigated wave scattering by multiple bottom-standing flexible porous barriers by employing the direct method and the wide-spacing approximation for various porous effect parameters. Das and Bora (2018) investigated the problem of obliquely incident wave damping by two fully submerged vertical parallel porous plates of different heights in finite depth water by employing eigenfunction expansion and least square method. Mohapatra et al. (2018) obtain the solution for surface gravity wave interaction with a submerged horizontal flexible porous plate based on Green's function in finite and infinite water depth.

Our aim in this study is to enhance understanding of whether including the effect of porosity on the problem of oblique wave scattering by two unequal partially immersed and submerged barriers in infinitely deep water is physically realistic. To the author's knowledge, no previous investigation has been conducted on the existence of water wave scattering by two unequal barriers in the presence of different porosity. The problem is split into three separate parts involving three potential functions that describe the resultant motion in the fluid region because of the geometrical symmetry of the unequal barriers, as conducted by Roy et al. (2016). To solve the problem, the potential function is reduced to linear integral equations by using the eigenfunction expansions along with the Havelock inversion formula followed by a matching process. The integral equations were approximated using single-term Galerkin approximations. The hydrodynamics quantities are then computed numerically using the numerical solution of integral equation. The reflection coefficient is represented graphically against the wave number for different parameters. When the value of the porous effect parameters is zero, the obtained results analytically match the corresponding results in Roy et al. (2016). The numerical estimate of reflection coefficient is depicted graphically against the wave number, neglecting effect of porosity, which agrees with the result obtained by Evans and Morris (1972) and Roy et al. (2016) for two equal and unequal partially immersed barriers, respectively. In the case of submerged barriers, graphs of $|R|$ against the wave number exactly match the graphs in Jarvis (1971) and Roy et al. (2016) for two equal and unequal rigid barriers, respectively. When the two porous barriers are closely spaced, the value of reflection coefficient reduces to those for a single porous barrier obtained by Manam and Sivanesan (2016). The graphs of $|R|$ against the wave number for different values of porosity almost coincide with the corresponding graphs in Manam and Sivanesan (2016) for a single immersed and submerged porous barrier. Numerical estimates for amount of dissipated energy and coefficient of wave force are obtained for various values of different parameters involved in the problem. Also, the computed results of reflection and transmission coefficients satisfy the energy identity for permeable and impermeable barriers. We have seen that porosity affects the reflection coefficient considerably. Moreover, in the presence of porosity, the length and the difference between two barriers affect the reflection and transmission coefficient substantially, and waves are completely transmitted for an infinite number of discrete wave frequencies for both cases.

2 Formulation of the Problem

Under the assumption of linearized theory, the problem is studied in a rectangular Cartesian coordinate system in which y-axis is taken vertically downwards along the fluid region $y \geq 0$. Let us consider two partially immersed porous barriers of different heights situated at $x = -l, y \in L_1 \equiv (0, a)$ (first porous barrier) and $x = l, y \in L_2 \equiv (0, b)$ (second porous barrier), and in the submerged case, barriers occupy the position $x = -l, y \in L_1 \equiv (a, \infty)$ (first porous barrier) and $x = l, y \in L_2 \equiv (b, \infty)$ (second porous barrier), where a and b are finite positive numbers (see Figs. 1 and 2). The fluid region is divided into three subregions, namely, region $-$ I $\equiv (-\infty < x < -l, 0 < y < \infty)$,

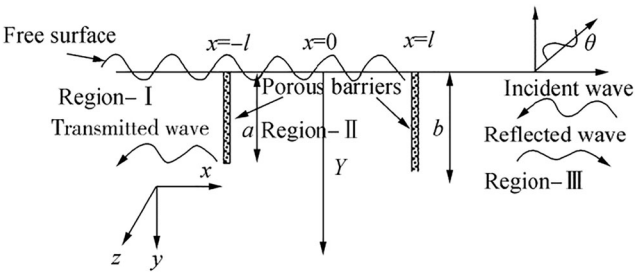

Fig. 1 Schematic for partially immersed porous barriers

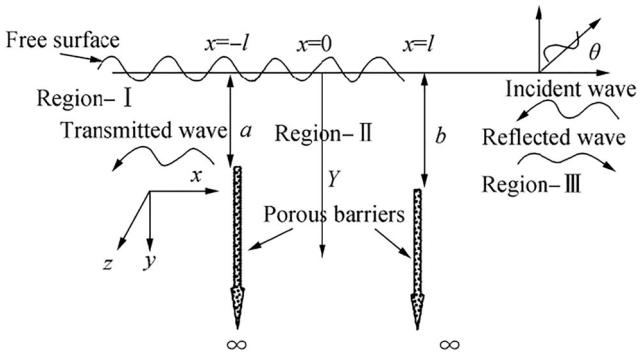

Fig. 2 Schematic for totally submerged porous barriers

region $-$ II $\equiv (-l < x < l, 0 < y < \infty)$, and region $-$ III $\equiv (l < x < \infty, 0 < y < \infty)$. The fluid is assumed to be incompressible, homogeneous, and inviscid, and the motion is irrotational and harmonic in time with angular frequency ω. Thus, the fluid motion is described by the velocity potential $\Phi_j(x, y, z, t)$ of the form $\Phi_j(x, y, z, t) = \mathrm{Re}\{\phi_j(x, y)e^{i\nu z - i\omega t}\}$ where $\phi_j(x, y)$ is the spatial component of the velocity potential, with Re denoting the real part, and ν is the component of the wave number along the z-axis. Here, the component ν is defined by $\nu = K \sin\theta$, where $K = \frac{\omega^2}{g}$, g is the acceleration due to gravity and θ is the angle of the incident wave to the x-axis. The spatial velocity potential in each subregion satisfies the Helmholtz equation

$$\left(\nabla^2 - \nu^2\right)\phi_j = 0 \quad \textit{in the fluid region}, \tag{1}$$

where $\nabla^2 = \partial^2/\partial x^2 + \partial^2/\partial y^2$. The free surface boundary condition is given by

$$K\phi_j + \frac{\partial \phi_j}{\partial y} = 0 \quad \text{on } y = 0 \tag{2}$$

The bottom boundary condition is given by

$$|\nabla\phi_j| \to 0, \quad \text{as } y \to \infty \textit{for deep water} \tag{3}$$

where $\nabla = (\partial/\partial x, \partial/\partial y)$.

The velocity potential is bounded everywhere in the fluid region except at the submerged sharp edge of the porous barrier edges $(-l, a)$ and (l, b). For the thin porous barriers, the edge condition may be obtained as (see Mandal and Chakrabarti 2000; Karp and Karal 1962)

$$|\nabla\phi_j| = O\left(r^{-\frac{1}{2}}\right) \quad \text{as } r \to 0 \tag{4}$$

where

$$r = \begin{cases} \sqrt{(x+l)^2 + (y-a)^2}, & \textit{for } L_1 \\ \sqrt{(x-l)^2 + (y-b)^2}, & \textit{for } L_2 \end{cases}$$

Aside from the preceding boundary conditions, the velocity potentials satisfy the following boundary conditions also at the interface of the three subregions:

$$\frac{\partial \phi_1}{\partial x} = \frac{\partial \phi_2}{\partial x} = -iKG_1(\phi_2 - \phi_1), \quad x = -l, \quad y \in L_1 \tag{5}$$

$$\frac{\partial \phi_1}{\partial x} = \frac{\partial \phi_2}{\partial x} \quad \textit{and} \quad \phi_1 = \phi_2, \quad x = -l, \quad y \in L_1 \tag{6}$$

$$\frac{\partial \phi_2}{\partial x} = \frac{\partial \phi_3}{\partial x} = -iKG_2(\phi_3 - \phi_2), \quad x = l, \quad y \in L_2 \tag{7}$$

$$\frac{\partial \phi_2}{\partial x} = \frac{\partial \phi_3}{\partial x} \quad \textit{and} \quad \phi_2 = \phi_3, \quad x = l, \quad y \in L_2 \tag{8}$$

where G_1 and G_2 are the dimensionless porous effect parameters of the two barriers and $L_j \equiv (0, \infty) - L_j, j = 1, 2$.

The conditions at infinity are given by

$$\phi(x, y) \sim \begin{cases} \phi_0(y)\left\{e^{-i\mu(x-l)} + Re^{i\mu(x+l)}\right\} & \text{as } x \to \infty \\ \phi_0(y)Te^{-i\mu(x-l)} & \text{as } x \to -\infty \end{cases} \tag{9}$$

where R and T are the unknown complex reflection and transmission coefficients to be determined, respectively, $\phi_0(y) = e^{-Ky}$, and $\mu = K\cos\theta$.

3 Solution Procedure

The velocity potentials $\phi_j(x, y)$ satisfy the Helmholtz equation in the fluid domain as in Eq. (1) along with the boundary conditions Eqs. (2) and (3). With the use of Havelock's expansion formula, the velocity potentials $\phi_j(x, y)$ for each of the three regions are given by

$$\phi_1(x, y) = T\phi_0(y)e^{-i\mu(x+l)} + \int_0^\infty \frac{A(k)S(k, y)}{t\left(k^2 + K^2\right)} e^{t(x+l)}\,dk \tag{10}$$

$$\phi_2(x, y) = \phi_0(y)\left(\alpha e^{i\mu x} + \beta e^{-i\mu x}\right) + \int_0^\infty \frac{\{B(k)e^{tx} + C(k)e^{-tx}\}S(k, y)}{t\left(k^2 + K^2\right)}\,dk \tag{11}$$

$$\phi_3(x, y) = \phi_0(y)\left\{e^{-i\mu(x-l)} + Re^{i\mu(x-l)}\right\} + \int_0^\infty \frac{D(k)S(k, y)}{t\left(k^2 + K^2\right)} e^{-t(x-l)}\,dk \tag{12}$$

where $t = \sqrt{k^2 + \nu^2}$, $S(k, y) = k\cos ky - K\sin ky$, α and β are arbitrary constants, and $A(k)$, $B(k)$, $C(k)$, and $D(k)$ are unknown functions of k. Given that the velocity potential is continuous across the gap at $x = \mp l$ for all y, we define the functions as follows:

$$u_1(y) = \frac{\partial \phi_1(-l, y)}{\partial x} = \frac{\partial \phi_2(-l, y)}{\partial x} \tag{13}$$

$$u_2(y) = \frac{\partial \phi_2(l,y)}{\partial x} = \frac{\partial \phi_3(l,y)}{\partial x} \tag{14}$$

We define the potential difference across the barriers at $x = \mp l$ as given by

$$v_1(y) = \phi_2(-l,y) - \phi_1(-l,y) \tag{15}$$

$$v_2(y) = \phi_3(l,y) - \phi_2(l,y) \tag{16}$$

Using the transmission boundary condition from Eqs. (5)–(8), along with Eqs. (13)–(16), we obtain

$$u_j(y) = -\mathrm{i}KG_j v_j(y), y \in L_j, \quad j = 1,2 \tag{17}$$

and

$$v_j(y) = 0, y \in L_j, j = 1,2. \tag{18}$$

Now, by using the expression of the velocity potential for three regions in Eqs. (10)–(12) along with the expression in Eqs. (13) and (14) for gap and applying Havelock's inversion formula, we obtain

$$T\mathrm{e}^{2i\mu l} = -\left(\alpha \mathrm{e}^{-i\mu l} - \beta \mathrm{e}^{i\mu l}\right) = \frac{2i}{\cos\theta} \int_{L_1} u_1(y)\phi_0(y)\mathrm{d}y \tag{19}$$

$$1 - R\mathrm{e}^{2i\mu l} = -\left(\alpha \mathrm{e}^{i\mu l} - \beta \mathrm{e}^{-i\mu l}\right) \frac{2i}{\cos\theta} \int_{L_2} u_2(y)\phi_0(y)\mathrm{d}y \tag{20}$$

$$\left.\begin{aligned} A(k) &= B(k)\mathrm{e}^{-tl} - C(k)\mathrm{e}^{tl} = \frac{2}{\pi}\int_{L_1} u_1(y)S(k,y)\mathrm{d}y \\ D(k) &= B(k)\mathrm{e}^{tl} - C(k)\mathrm{e}^{-tl} = \frac{2}{\pi}\int_{L_2} u_2(y)S(k,y)\mathrm{d}y \end{aligned}\right\} \tag{21}$$

By using the expression of the velocity potential for three regions from Eqs. (10)–(12) along with the expression in Eqs. (13) and (14), along the barriers and applying Havelock's inversion formula, we obtain

$$\alpha \mathrm{e}^{-i\mu l} + \beta \mathrm{e}^{i\mu l} - T\mathrm{e}^{2i\mu l} = 2K\int_{L_1} v_1(y)\phi_0(y)\mathrm{d}y \tag{22}$$

$$1 + R\mathrm{e}^{2i\mu l} - \alpha \mathrm{e}^{i\mu l} - \beta \mathrm{e}^{-i\mu l} = 2K\int_{L_2} v_2(y)\phi_0(y)\mathrm{d}y \tag{23}$$

$$\left.\begin{aligned} B(k)\mathrm{e}^{-tl} + C(k)\mathrm{e}^{tl} - A(k) &= \frac{2t}{\pi}\int_{L_1} v_1(y)S(k,y)\mathrm{d}y \\ D(k) = B(k)\mathrm{e}^{tl} + C(k)\mathrm{e}^{-tl} &= -\frac{2t}{\pi}\int_{L_2} v_2(y)S(k,y)\mathrm{d}y \end{aligned}\right\} \tag{24}$$

The constants α and β can be found in the terms of R and T, using the first two terms of Eqs. (19) and (20) as

$$\left.\begin{aligned} \alpha &= \frac{i}{2}\mathrm{cosec}(2\mu l)\mathrm{e}^{i\mu l}\left\{1 - R\mathrm{e}^{2i\mu l} - T\right\} \\ \beta &= \frac{i}{2}\mathrm{cosec}(2\mu l)\mathrm{e}^{-i\mu l}\left\{1 - R\mathrm{e}^{2i\mu l} - T\mathrm{e}^{4i\mu l}\right\} \end{aligned}\right\} \tag{25}$$

Now, we find the expression of $B(k)$ and $C(k)$ in terms of $A(k)$ and $D(k)$ using the first two terms of the first and second equations of Eq. (21) as follows:

$$\begin{bmatrix} B(k) \\ C(k) \end{bmatrix} = \frac{1}{2\sinh(2tl)} \begin{bmatrix} D(k)\mathrm{e}^{tl} - A(k)\mathrm{e}^{-tl} \\ D(k)\mathrm{e}^{-tl} - A(k)\mathrm{e}^{tl} \end{bmatrix} \tag{26}$$

With the use of the expression of α and β from Eq. (25), Eqs. (22) and (23) reduce to

$$i\mathrm{csc}(2\mu l)\left\{1 - R\mathrm{e}^{2i\mu l} - T\right\} = 2K\int_{L_1} v_1(y)\phi_0(y)\mathrm{d}y \tag{27}$$

$$i\mathrm{csc}(2\mu l)\left\{R - \mathrm{e}^{2i\mu l} + T\mathrm{e}^{2i\mu l}\right\} = 2K\int_{L_2} v_2(y)\phi_0(y)\mathrm{d}y \tag{28}$$

With the use of the expression of $B(k)$ and $C(k)$ from Eq. (26), the two equations of Eq. (24) reduce to

$$\begin{bmatrix} \dfrac{D(k) - A(k)\mathrm{e}^{2tl}}{\sinh(2tl)} \\ \dfrac{D(k)\mathrm{e}^{2tl} - A(k)}{\sinh(2tl)} \end{bmatrix} = \frac{2t}{\pi} \begin{bmatrix} \int_{L_1} v_1(y)S(k,y)\mathrm{d}y \\ -\int_{L_2} v_2(y)S(k,y)\mathrm{d}y \end{bmatrix} \tag{29}$$

Now, we simplify Eq. (29) to find the expressions of $A(k)$ and $D(k)$ in terms of the functions $v_j(y)$ $(j = 1, 2)$ as given by

$$\begin{bmatrix} A(k) \\ D(k) \end{bmatrix} = -\frac{t}{\pi} \begin{bmatrix} \int_{L_1} v_1(y)S(k,y)\mathrm{d}y \\ +\int_{L_2} \mathrm{e}^{-2tl} v_2(y)S(k,y)\mathrm{d}y \\ \int_{L_1} \mathrm{e}^{-2tl} v_1(y)S(k,y)\mathrm{d}y \\ +\int_{L_2} v_2(y)S(k,y)\mathrm{d}y \end{bmatrix} \tag{30}$$

Now, by substituting the expressions of $A(k)$ and $D(k)$ from Eq. (30) in the expression of $u_1(y)$ and $u_2(y)$ and using the relation (17), we obtain the following integral equations in $v_j(y)$ $(j = 1, 2)$:

$$\begin{aligned} &i\mu T\mathrm{e}^{2i\mu l}\phi_0(y) + \int_{L_1} v_1(z)\mathcal{K}_1(y,z)\mathrm{d}z \\ &+ \int_{L_2} v_2(z)\mathcal{K}_2(y,z)\mathrm{d}z = iKG_1 v_1(y), y \in L_1 \end{aligned} \tag{31}$$

$$\begin{aligned} &i\mu(1 - R\mathrm{e}^{2i\mu l})\phi_0(y) + \int_{L_1} v_1(z)\mathcal{K}_2(y,z)\mathrm{d}z \\ &+ \int_{L_2} v_2(z)\mathcal{K}_1(y,z)\mathrm{d}z = iKG_2 v_2(y), y \in L_2 \end{aligned} \tag{32}$$

where

$$\left.\begin{aligned} \mathcal{K}_1(y,z) &= \frac{1}{\pi}\int_0^\infty \frac{tS(k,z)S(k,y)}{k^2 + K^2}\mathrm{d}k \\ \mathcal{K}_2(y,z) &= \frac{1}{\pi}\int_0^\infty \frac{t\mathrm{e}^{-2tl}S(k,z)S(k,y)}{k^2 + K^2}\mathrm{d}k \end{aligned}\right\} \tag{33}$$

Now, the above integral Eqs. (31) and (32) can be written in a single integral equation as follows:

$$\begin{aligned} &-i\mu(E_j - F_j)\phi_0(y) + \int_{L_j} v_j(z)\mathcal{K}_1(y,z)\mathrm{d}z \\ &+ \int_{L_{3-j}} v_{3-j}(z)\mathcal{K}_1(y,z)\mathrm{d}z = iKG_j v_j(y), \\ &y \in L_j, j = 1,2 \end{aligned} \tag{34}$$

where $E_1 = 0$, $E_2 = -1$, $F_1 = T\mathrm{e}^{2i\mu l}$, and $F_2 = -R\mathrm{e}^{2i\mu l}$.

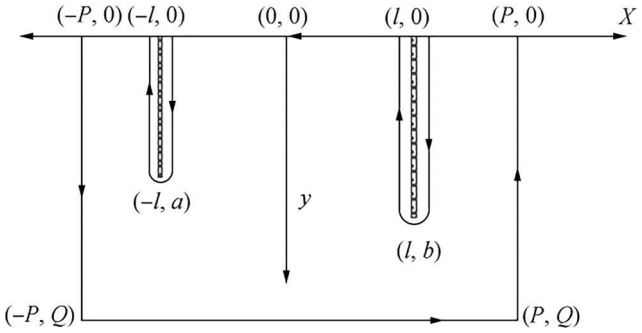

Fig. 3 Contour for partially immersed porous barriers

With the use of the matrix notation, the integral Eq. (34) can be expressed as a compact matrix form as follows:

$$-i\mu \boldsymbol{H}(y)(\boldsymbol{E}-\boldsymbol{F})\phi_0(y) + \int_0^\infty N(y,z)v(z)\mathrm{d}z = iKGH(y)v(y), y\in(0,\infty) \tag{35}$$

in which

$$\boldsymbol{E} = [E_1 E_2]^{\mathrm{T}},$$
$$\boldsymbol{F} = [F_1 F_2]^{\mathrm{T}},$$
$$\boldsymbol{v}(y) = [v_1(y) v_2(y)]^{\mathrm{T}},$$
$$\boldsymbol{G} = [G_1 G_2]^{\mathrm{T}},$$
$$\boldsymbol{H}(y) = \begin{bmatrix} H_1(y) & 0 \\ 0 & H_2(y) \end{bmatrix},$$
$$\boldsymbol{\mathcal{K}}(y,z) = \begin{bmatrix} \mathcal{K}_1(y,z) & \mathcal{K}_2(y,z) \\ \mathcal{K}_2(y,z) & \mathcal{K}_1(y,z) \end{bmatrix},$$

where

$$H_j(y) = \begin{cases} 1 & y \in L_j, \\ 0 & y \in \overline{L}_j, \end{cases} \quad j = 1,2$$
$$N(y,z) = \boldsymbol{H}(y)\boldsymbol{\mathcal{K}}(y,z)\boldsymbol{H}(z)$$

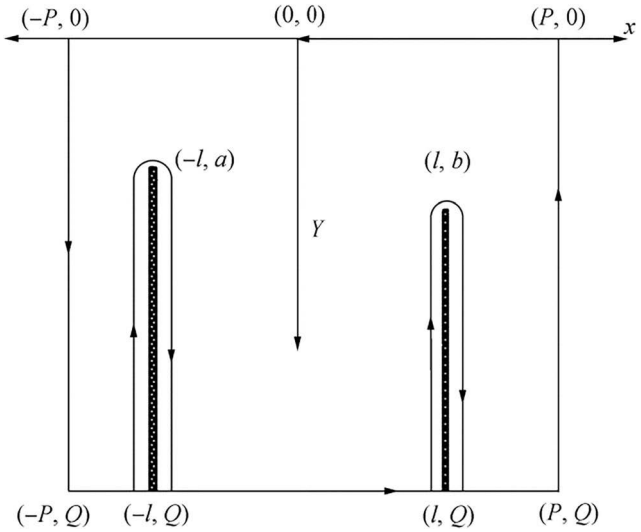

Fig. 4 Contour for totally submerged porous barriers

Now, we introduce a 2 × 2 matrix as follows:

$$\boldsymbol{V}(z) = \begin{bmatrix} V_1^1(z) & V_1^2(z) \\ V_2^1(z) & V_2^2(z) \end{bmatrix}$$

as $v(z) = i\mu V(z)(\boldsymbol{E}-\boldsymbol{F})$.

With the use of the expression of $v(z)$, the integral Eq. (35) is transformed into the following equation:

$$\int_0^\infty N(y,z)\boldsymbol{V}(z)\mathrm{d}z - iKGH(y)V(y) = \boldsymbol{H}(y)\phi_0(y), y\in(0,\infty) \tag{36}$$

The above matrix Eq. (36) is equivalent to the following integral equations:

$$\int_{L_j} \mathcal{K}_1(y,z)V_j^m(z)\mathrm{d}z + \int_{L_{3-j}} \mathcal{K}_2(y,z)V_{3-j}^m(z) - iKG_jV_j^m(y) = \lambda_m^j\phi_0(y), \quad y \in L_j;\ m,j = 1,2 \tag{37}$$

where

$$\lambda_m^j = \begin{cases} 1 & j = m \\ 0 & j \neq m \end{cases}$$

Using the constants of E_j and F_j, we combine Eqs. (27) and (28) of the form as

$$i\csc(2\mu l)\left[E_j\mathrm{e}^{2i\mu l} - F_j\mathrm{e}^{-2i\mu l} - E_{3-j} + F_{3-j}\right] = 2K\int_{L_j} v_j(y)\phi_0(y)\mathrm{d}y, \quad j = 1,2 \tag{38}$$

With the use of the matrix notation, the integral Eq. (38) can be written in a compact matrix form as given by

$$\int_0^\infty H(z)v(z)\phi_0(z)\mathrm{d}z = \frac{i}{2K}\mathrm{cosec}(2\mu l)\left(\boldsymbol{DE}-\boldsymbol{DF}\right) \tag{39}$$

where $\boldsymbol{D} = \begin{bmatrix} \mathrm{e}^{2i\mu l} & -1 \\ -1 & \mathrm{e}^{2i\mu l} \end{bmatrix}, \boldsymbol{D} = \begin{bmatrix} \mathrm{e}^{-2i\mu l} & -1 \\ -1 & \mathrm{e}^{-2i\mu l} \end{bmatrix}$.

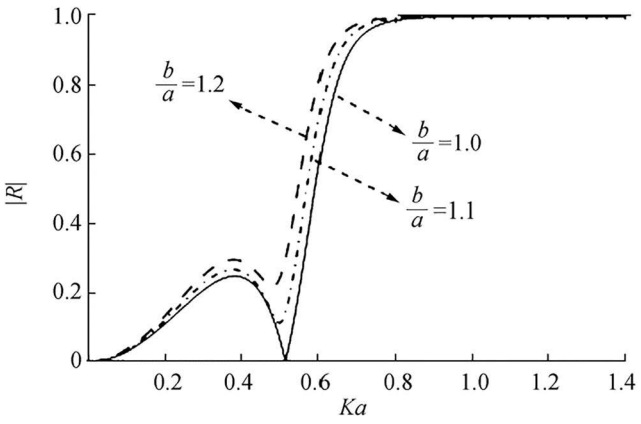

Fig. 5 Reflection coefficients for two partially immersed vertical barriers, for different values of $\frac{b}{a}(= 1, 1.1, 1.2)$ and a fixed value of $\theta = 0^{\mathrm{o}}$, $G_1 = G_2 = 0$, and $\frac{l}{a} = 1$

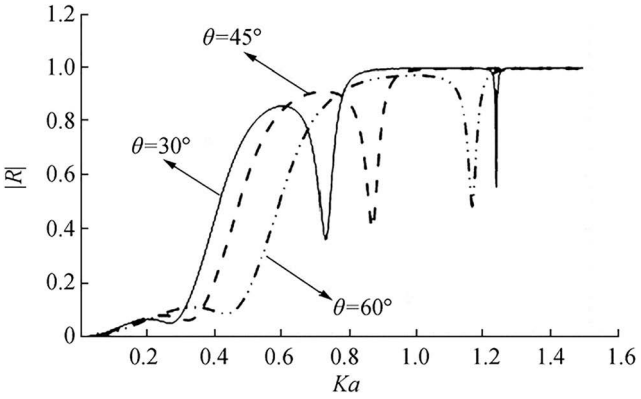

Fig. 6 Reflection coefficients for two partially immersed vertical barriers, for different values of $\theta(=30°, 45°, 60°)$ and a fixed value of $\frac{b}{a} = 1.2$, $G_1 = G_2 = 0$, and $\frac{l}{a} = 3$

With the use of the expression of $v(z) = i\mu V(z)(\boldsymbol{E} - \boldsymbol{F})$, the integral Eq. (39) transforms into

$$2K\mu(\boldsymbol{E}-\boldsymbol{F})S = \operatorname{csc}(2\mu l)\left(\boldsymbol{DE}-\boldsymbol{DF}\right) \tag{40}$$

where $S = \int_0^\infty H(z)\boldsymbol{V}(z)\phi_0(z)\mathrm{d}z$

Thus, the reflection and transmission coefficients are obtained as

$$\begin{bmatrix} T\mathrm{e}^{2i\mu l} \\ -R\mathrm{e}^{2i\mu l} \end{bmatrix} = Y\boldsymbol{E} \tag{41}$$

where $Y = [2K\mu S - \operatorname{csc}(2\mu l)\boldsymbol{D}]^{-1}[2K\mu S - \operatorname{csc}(2\mu l)\boldsymbol{D}]$.

To determine the reflection and transmission coefficients, we have to find the value of S. The solution of the integral expression of S can be obtained using the solution $\boldsymbol{V}(z)$ of the integral Eq. (36).

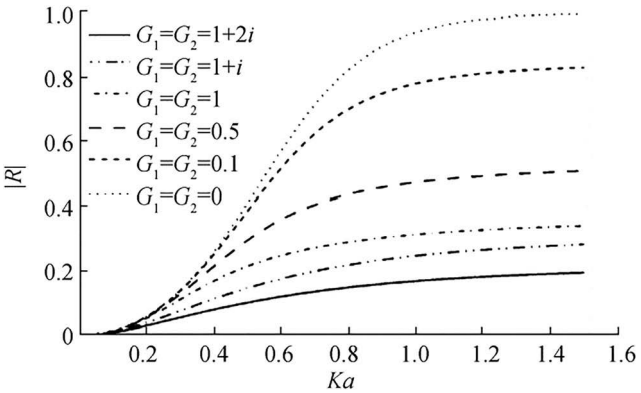

Fig. 7 Reflection coefficient for a partially immersed vertical barrier, for different values of $G_1 = G_2 = 0$, $G_1 = G_2 = 0.1$, $G_1 = 1 = G_2 = 0.5$, $G_1 = G_2 = 1$, $G_1 = G_2 = 1 + i$, $G_1 = G_2 = 1 + 2i$ and a fixed value of $\theta = 0°$, $\frac{b}{a} = 1$, and $\frac{l}{a} \to 0$

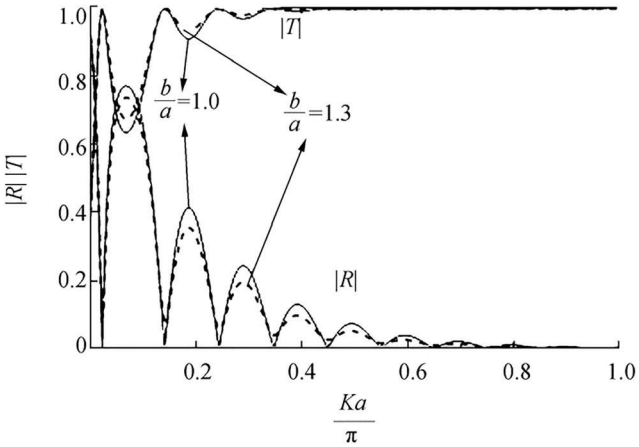

Fig. 8 Reflection and transmission coefficients for two submerged barriers, for different values of $\frac{b}{a} = (1, 1.3)$ and a fixed value of $\theta = 0°$, $G_1 = G_2 = 0$, and $\frac{l}{a} = 5$

3.1 For Partially Immersed Barriers

In this subsection, to construct a solution of the integral Eq. (36), we use single-term Galerkin approximation. We approximate the function $V_j^m(y)$ as given by

$$V_j^m(y) \simeq c_{jm} f_j(y), \quad j, m = 1, 2 \tag{42}$$

where $f_1(y)$ and $f_2(y)$ are Ursell's (1947) exact solution for the potential difference across a single barrier partially immersed up to depths a and b, respectively, and are given by

$$f_1(y) = \mathrm{e}^{-Ky}\int_a^y \frac{z\mathrm{e}^{Kz}}{\sqrt{a^2 - z^2}}\mathrm{d}z, \quad 0 < y < a \tag{43}$$

$$f_2(y) = \mathrm{e}^{-Ky}\int_b^y \frac{z\mathrm{e}^{Kz}}{\sqrt{b^2 - z^2}}\mathrm{d}z, \quad 0 < y < b \tag{44}$$

and $c_{jm}(j, m = 1, 2)$ are unknown constants to be determined. To determine the value of the unknown constants $c_{jm}(j, m = 1, 2)$, we substitute the expression $V_j^m(y)$ from Eq. (42) along with the expressions $f_1(y)$ and $f_2(y)$ into Eq. (37) and obtain the

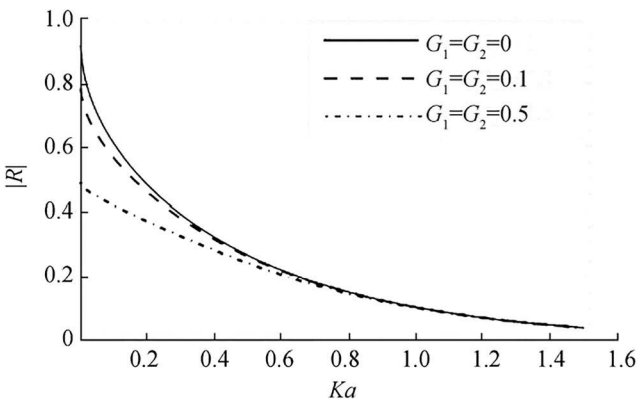

Fig. 9 Reflection coefficient for a submerged barrier, for different values of $G_1 = G_2 = (0, 0.1, 0.5)$ and a fixed value of $\theta = 0°$, $\frac{b}{a} = 1$, and $\frac{l}{a} \to 0$

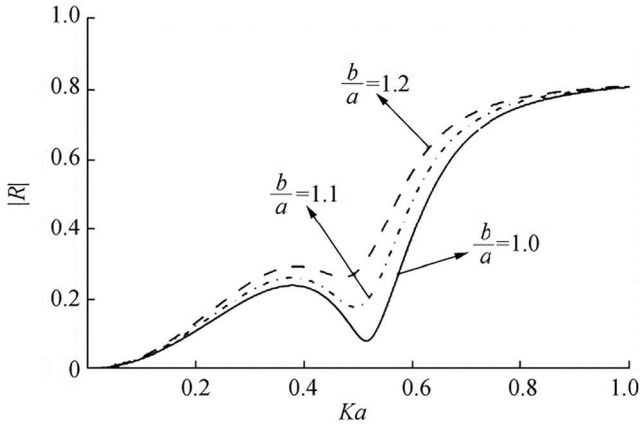

Fig. 10 Reflection coefficient for two partially immersed vertical barriers, for different values of $\frac{b}{a}(=1, 1.1, 1.2)$ and a fixed value of $G_1 = G_2 = 0.1$, $\frac{l}{a} = 1$, and $\theta = 0°$

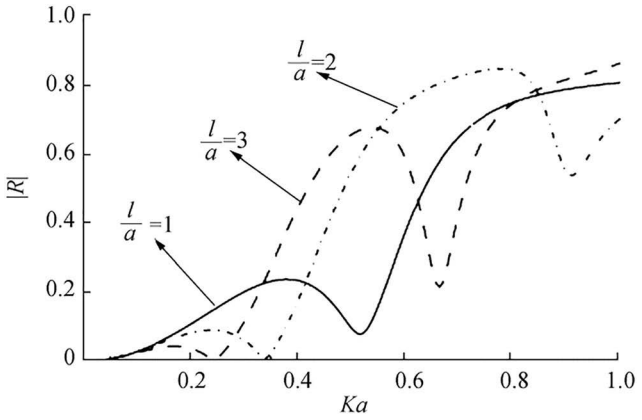

Fig. 12 Reflection coefficient for two partially immersed vertical barriers, for different values of $\frac{l}{a}(=1, 2, 3)$ and a fixed value of $G_1 = G_2 = 0.1$, $\frac{b}{a} = 1$, and $\theta = 0°$

following system of equations:

$$\left.\begin{aligned} c_{1m}\mathcal{M}_{11} + c_{2i}\mathcal{M}_{21} &= \lambda_1^m P_1, \quad m = 1,2 \\ c_{1m}\mathcal{M}_{12} + c_{2m}\mathcal{M}_{22} &= \lambda_2^m P_2, \quad m = 1,2 \end{aligned}\right\} \tag{45}$$

where

$$\left.\begin{aligned} &\mathcal{M}_{jj} = \int_{L_j} f_j(y)\left[\int_{L_j} \mathcal{K}_1(y,z) f_j(z)\mathrm{d}z\right]\mathrm{d}y \\ &-iKG_j \int_{L_j} [f_j(y)]^2 \mathrm{d}y, j = 1,2 \\ &\mathcal{M}_{jm} = \int_{L_j} f_j(y)\left[\int_{L_m} \mathcal{K}_2(y,z) f_m(z)\mathrm{d}z\right]\mathrm{d}y \\ &m, j = 1,2\ (j \neq m) \\ &P_j = \int_{L_j} \mathrm{e}^{-Ky} f_j(y)\mathrm{d}y,\ j = 1,2 \end{aligned}\right\} \tag{46}$$

Now, by placing the expressions of $f_1(z)$ and $f_2(z)$ from Eqs. (43) and (44) in the three equations of Eq. (46), we obtain

$$\mathcal{M}_{11} = \frac{\pi}{4}a^2 \int_0^\infty \frac{tJ_1^2(ka)}{k^2 + K^2}\mathrm{d}k - iKG_1 \int_0^a [f_1(y)]^2 \mathrm{d}y$$

$$\mathcal{M}_{22} = \frac{\pi}{4}b^2 \int_0^\infty \frac{tJ_1^2(kb)}{k^2 + K^2}\mathrm{d}k - iKG_2 \int_0^b [f_2(y)]^2 \mathrm{d}y$$

$$\mathcal{M}_{12} = \mathcal{M}_{21} = \frac{\pi}{4}ab \int_0^\infty \frac{t\mathrm{e}^{-2tl} J_1(ka) J_1(kb)}{k^2 + K^2}\mathrm{d}k$$

$$P_1 = -\frac{\pi a}{2K} I_1(Ka), P_2 = -\frac{\pi b}{2K} I_1(Kb)$$

where $J_1(.)$ is a Bessel function of the first kind of first order and $I_1(.)$ is a modified Bessel function of the first kind of first order. If $S = \{S_{jm}\}_{2\times 2}$, then we find S after substituting the expression from Eq. (42).

$$S_{jm} \simeq \int_{L_j} V_j^m(z)\mathrm{e}^{-Kz}\mathrm{d}z = c_{jm}P_j,\ \ j, m = 1,2 \tag{47}$$

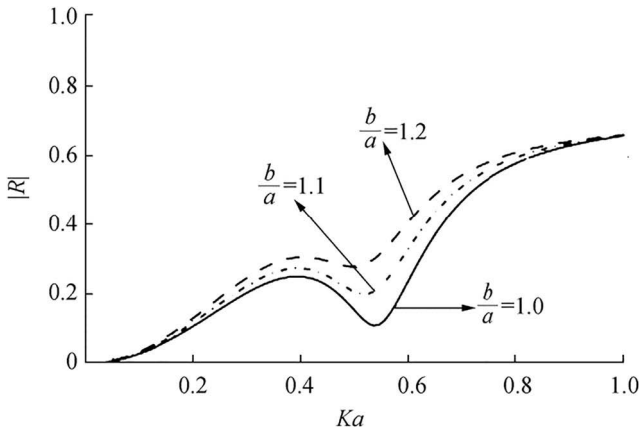

Fig. 11 Reflection coefficient for two partially immersed vertical barriers, for different values of $\frac{b}{a}(=1, 1.1, 1.2)$ and a fixed value of $G_1 = 0.1$, $G_2 = 0.2$, $\frac{l}{a} = 1$, and $\theta = 0°$

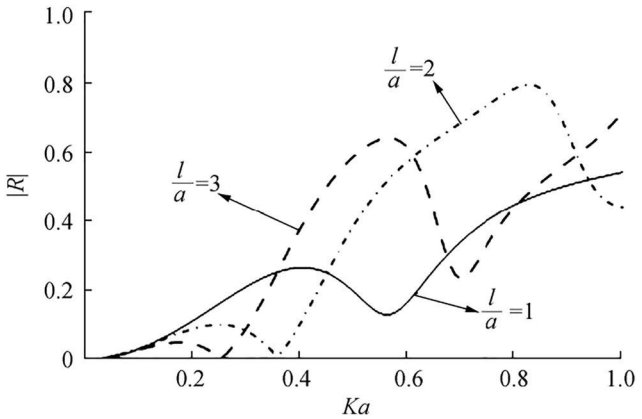

Fig. 13 Reflection coefficient for two partially immersed vertical barriers, for different values of $\frac{l}{a}(=1, 2, 3)$ and a fixed value of $G_1 = 0.1$, $G_2 = 0.3$, $\frac{b}{a} = 1$, and $\theta = 0°$

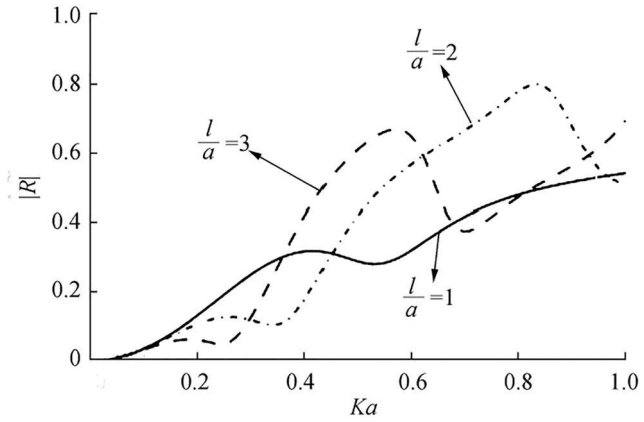

Fig. 14 Reflection coefficient for two partially immersed vertical barriers, for different values of $\frac{l}{a}(=1,2,3)$ and a fixed value of $G_1 = 0.1$, $G_2 = 0.3$, $\frac{b}{a} = 1.2$, and $\theta = 0°$

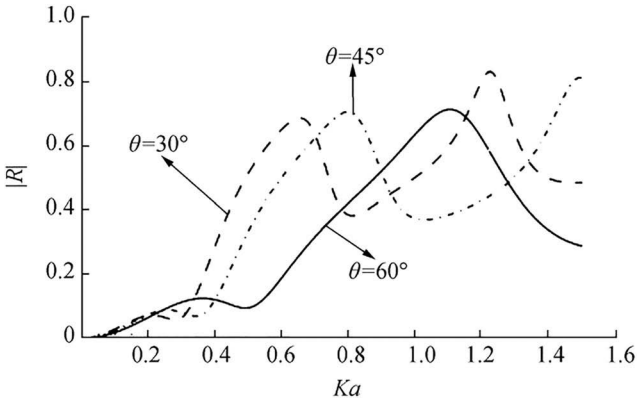

Fig. 16 Reflection coefficient for two partially immersed vertical barriers, for different values of $\theta(=30°, 45°, 60°)$ and a fixed value of $G_1 = 0.1$, $G_2 = 0.3$, $\frac{b}{a} = 1.2$, and $\frac{l}{a} = 3$

3.2 For Submerged Barriers

In this subsection, to construct a solution for the integral Eq. (36), we apply the same method as above and choose $L_1 = (a, \infty)$ and $L_2 = (b, \infty)$. We approximate the function $V_j^m(y)$ as given by

$$V_j^m(y) \simeq c_{jm} f_j(y), \quad j, m = 1, 2 \tag{48}$$

where $f_1(y)$ and $f_2(y)$ are given by

$$f_1(y) = \mathrm{e}^{-Ky} \int_a^y \frac{z\mathrm{e}^{Kz}}{\sqrt{z^2 - a^2}} \mathrm{d}z, \quad y > a \tag{49}$$

$$f_2(y) = \mathrm{e}^{-Ky} \int_b^y \frac{z\mathrm{e}^{Kz}}{\sqrt{z^2 - b^2}} \mathrm{d}z, \quad y > b \tag{50}$$

Here, we obtain

$$\mathcal{M}_{11} = \frac{\pi}{4} a^2 \int_0^\infty \frac{t J_0^2(ka)}{k^2 + K^2} \mathrm{d}k - iKG_1 \int_a^\infty [f_1(y)]^2 \mathrm{d}y$$

$$\mathcal{M}_{22} = \frac{\pi}{4} b^2 \int_0^\infty \frac{t J_0^2(kb)}{k^2 + K^2} \mathrm{d}k - iKG_2 \int_b^\infty [f_2(y)]^2 \mathrm{d}y$$

$$\mathcal{M}_{12} = \mathcal{M}_{21} = \frac{\pi}{4} ab \int_0^\infty \frac{t\mathrm{e}^{-2tl} J_0(ka) J_0(kb)}{k^2 + K^2} \mathrm{d}k$$

$$P_1 = \frac{a}{2K} K_0(Ka), \; P_2 = \frac{b}{2K} K_0(Kb)$$

where $J_0(.)$ is a Bessel function of the first kind of zero order and $K_0(.)$ is a modified Bessel function of the second kind of zero order. The same steps as in the case of partially immersed barriers are followed to determine S approximately.

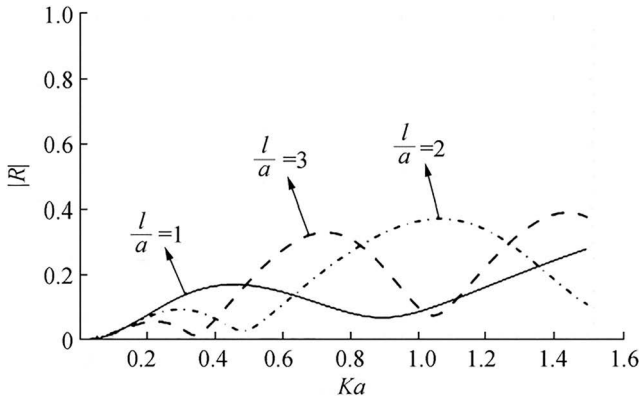

Fig. 15 Reflection coefficient for two partially immersed vertical barriers, for different values of $\frac{l}{a}(=1,2,3)$ and a fixed value of $G_1 = 1$, $G_2 = 1 + 0.5i$, $\frac{b}{a} = 1.2$, and $\theta = 45°$

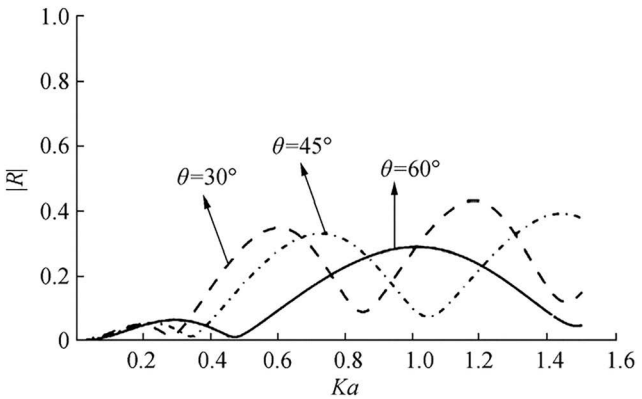

Fig. 17 Reflection coefficient for two partially immersed vertical barriers, for different values of $\theta(=30°, 45°, 60°)$ and a fixed value of $G_1 = 1$, $G_2 = 1 + 0.5i$, $\frac{b}{a} = 1.2$, and $\frac{l}{a} = 3$

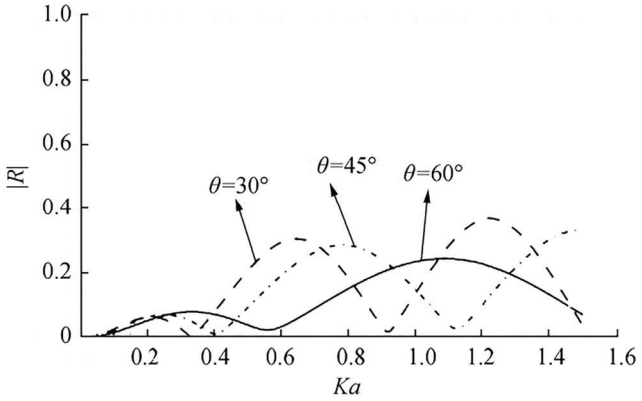

Fig. 18 Reflection coefficient for two partially immersed vertical barriers, for different values of $\theta(=30°, 45°, 60°)$ and a fixed value of $G_1 = 1$, $G_2 = 2$, $\frac{b}{a} = 1.2$, and $\frac{l}{a} = 3$

4 Energy Identity

In this section, we determined the energy dissipation due to the effect of the porosity of barriers by using Green's integral theorem to the function $\phi(x, y)$ and its complex conjugate $\phi(x, y)$ in the fluid region bounded by the lines $y = 0$ $(l \le x \le P)$; $x = l \pm 0$ $(0 \le y \le b)$; $y = 0$ $(-l \le x \le l)$; $x = -l \pm 0$ $(0 \le y \le a)$; $y = 0$ $(-P \le x \le -l)$; $x = -P (0 \le y \le Q)$; $y = Q(-P \le x \le P)$; $x = P(0 \le y \le Q)$ for partially immersed case and $y = 0$ $(-P \le x \le P)$; $x = -P(0 \le y \le Q)$; $y = Q(-P \le x \le -l)$; $x = -l \pm 0$ $(a \le y \le Q)$; $y = Q(-l \le x \le l)$; $x = l \pm 0 (b \le y \le Q)$; $y = Q(l \le x \le P)$; $x = P(0 \le y \le Q)$ for submerged case and internally by circles with a small radius ϵ with center at $(-l, a)$ and (l, b) (see Figs. 3 and 4). Finally, by making $P, Q \to \infty$ and $\epsilon \to 0$, we calculate the energy identity as follows

$$|R|^2 + |T|^2 = 1 - J \tag{51}$$

where

$$J = \frac{2K^2}{\mu} \sum_{i=1}^{2} \mathrm{Re}(G_i) \int_{L_i} \left|\phi_{i+1} - \phi_i\right|^2 dy$$

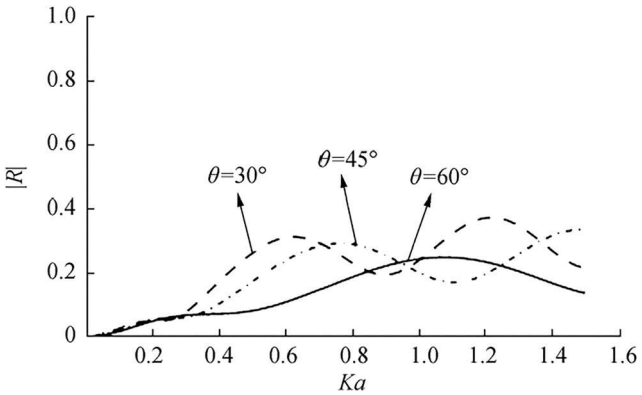

Fig. 19 Reflection coefficient for two partially immersed vertical barriers, for different values of $\theta(=30°, 45°, 60°)$ and a fixed value of $G_1 = 2$, $G_2 = 1$, $\frac{b}{a} = 1.2$, and $\frac{l}{a} = 3$

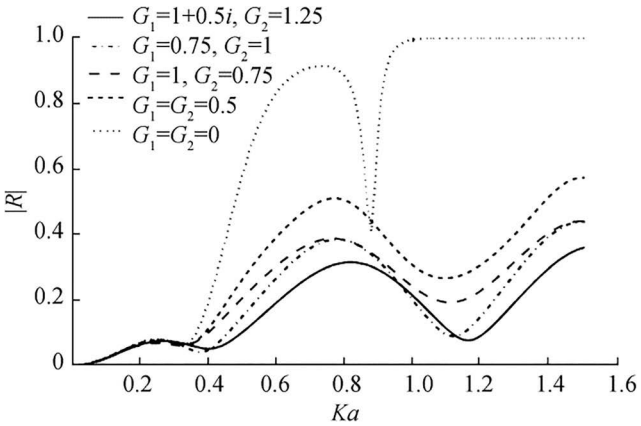

Fig. 20 Reflection coefficient for two partially immersed vertical barriers, for different values of $G_1 = G_2 = 0$; $G_1 = G_2 = 0.5$; $G_1 = 1$, $G_2 = 0.75$; $G_1 = 0.75$, $G_2 = 1$; $G_1 = 1 + 0.5i$, $G_2 = 1.25$ and a fixed value of $\theta = 45°$, $\frac{b}{a} = 1.2$, and $\frac{l}{a} = 3$

and $\mathrm{Re}(G_i)$ is the real part of the porous effect parameters. Clearly, the integral part of the expression of J is always positive. Therefore, we can conclude that $|R|^2 + |T|^2 < 1$. If the barriers are impermeable $(G_1 = G_2 = 0)$, then the energy dissipation coefficient is always zero.

5 Dynamic Force

The linear Bernoulli equation of the dynamic pressure jump on the two porous barriers can be written in the form (see Li et al. 2015)

$$P(x, y) = i\rho\omega\left\{(\phi_1 - \phi_2)_{x=-l} + (\phi_2 - \phi_3)_{x=l}\right\} \tag{52}$$

where ρ is the water density. Now, by integrating the dynamic pressure jump along the porous barriers, we obtain the magnitude of the horizontal wave force acting on the barriers, as given (Li et al. 2015)

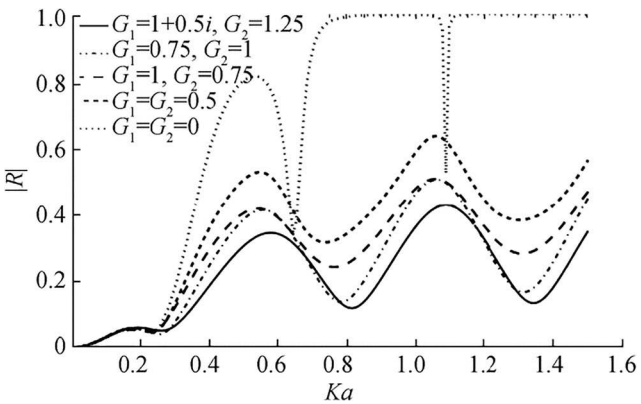

Fig. 21 Reflection coefficient for two partially immersed vertical barriers, for different values of $G_1 = G_2 = 0$; $G_1 = G_2 = 0.5$; $G_1 = 1$, $G_2 = 0.75$; $G_1 = 0.75$, $G_2 = 1$; $G_1 = 1 + 0.5i$, $G_2 = 1.25$ and a fixed value of $\theta = 0°$, $\frac{b}{a} = 1.2$, and $\frac{l}{a} = 3$

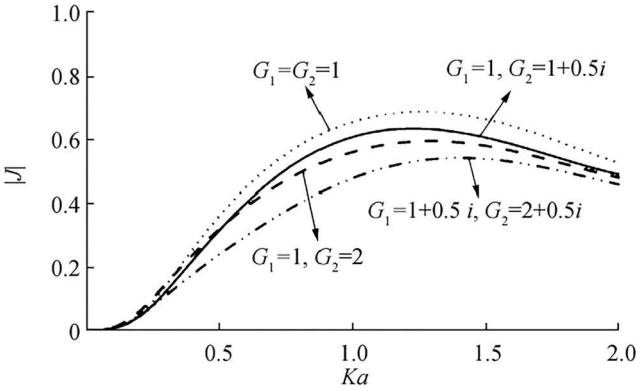

Fig. 22 Dissipated energy for two partially immersed vertical barriers, for different values of $G_1 = G_2 = 1$; $G_1 = 1$, $G_2 = 2$; $G_1 = 1$, $G_2 = 1 + 0.5i$; $G_1 = 1 + 0.5i$, $G_2 = 2 + 0.5i$ and a fixed value of $\theta = 45°$, $\frac{b}{a} = 1$, and $\frac{l}{a} = 1$

$$C_f = i\rho\omega\sum_{i=1}^{2}\int_{L_i}\left(\phi_i - \phi_{i+1}\right)\mathrm{d}y \tag{53}$$

The nondimensional form of the horizontal force coefficient on the vertical porous barriers is given by

$$K_f = \frac{K|C_f|}{\rho g} \tag{54}$$

6 Numerical Results

In this section, we found the numerical solution of the reflection and transmission coefficients, amount of dissipated energy, and wave force. To find all the hydrodynamics quantities, we first approximate the integral expression S. After approximating the integral expression of S, the reflection and transmission coefficients are computed numerically from Eq. (41) for various values of different dimensionless parameters, and they are presented graphically.

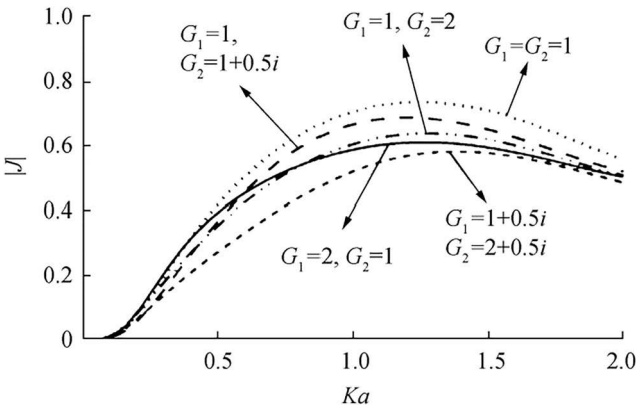

Fig. 23 Dissipated energy for two partially immersed vertical barriers, for different values of $G_1 = G_2 = 1$; $G_1 = 1$, $G_2 = 2$; $G_1 = 2$, $G_2 = 1$; $G_1 = 1$, $G_2 = 1 + 0.5i$; $G_1 = 1 + 0.5i$, $G_2 = 2 + 0.5i$ and a fixed value of $\theta = 45°$, $\frac{b}{a} = 1.3$, and $\frac{l}{a} = 1$

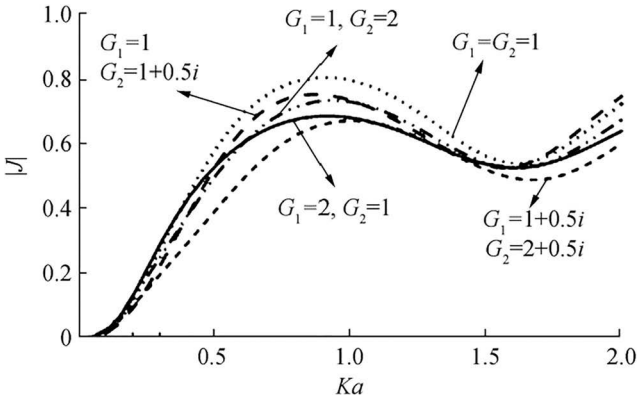

Fig. 24 Dissipated energy for two partially immersed vertical barriers, for different values of $G_1 = G_2 = 1$; $G_1 = 1$, $G_2 = 2$; $G_1 = 2$, $G_2 = 1$; $G_1 = 1$, $G_2 = 1 + 0.5i$; $G_1 = 1 + 0.5i$, $G_2 = 2 + 0.5i$ and a fixed value of $\theta = 0°$, $\frac{b}{a} = 1.3$, and $\frac{l}{a} = 1$

6.1 Approximation to Existing Results

In this section, we compared the present results with the corresponding cases available in the literature. To validate the current results, we take $G_1 = G_2 = 0$ in Eqs. (5) and (7), and the corresponding problems exactly match the one considered by Roy et al. (2016). A numerical study for a single rigid vertical barrier is shown in Fig. 5 for three different values of $\frac{b}{a}(= 1, 1.1, 1.2)$ and a fixed value of $\theta = 0$, $G_1 = G_2 = 0$, and $\frac{l}{a} = 1$. For the case of two identical partially immersed barriers ($b/a = 1$), the curve of $|R|$ in Fig. 5 coincides with the curve in Fig. 1 of Evans and Morris (1972). For the case of two nonidentical partially immersed barriers ($b/a = 1.1, 1.2$), the curves of $|R|$ in Fig. 5 agree with the curves in Fig. 1 of Roy et al. (2016). The good agreement between the results validates the current formulation of the problem. In Fig. 6, graphs of $|R|$ are plotted against the wave number Ka for different values of $\theta(=30°, 45°, 60°)$ and a fixed value of $\frac{b}{a} = 1.2$, $G_1 = G_2 = 0$, and $\frac{l}{a} = 3$. Zeros of $|R|$ are never possible for nonuniform partially immersed barriers in the case of

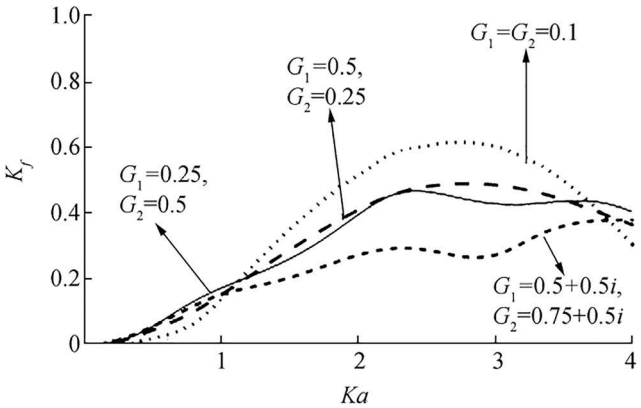

Fig. 25 Wave force for two partially immersed vertical barriers, for different values of $G_1 = G_2 = 0.1$; $G_1 = 0.25$, $G_2 = 0.5$; $G_1 = 0.5$, $G_2 = 0.25$; $G_1 = 0.5 + 0.5i$, $G_2 = 0.75 + 0.5i$ and a fixed value of $\theta = 45°$, $\frac{b}{a} = 1$, and $\frac{l}{a} = 1$

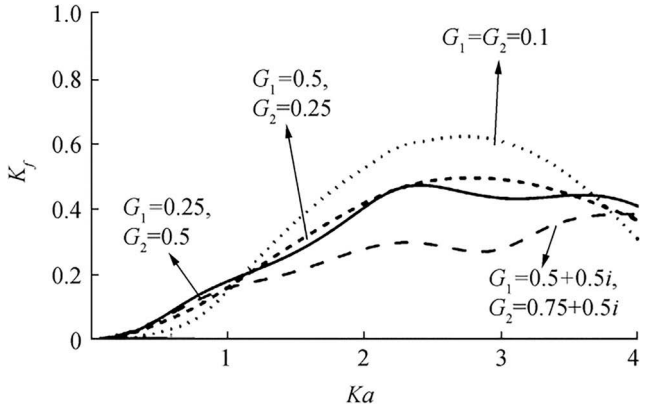

Fig. 26 Wave force for two partially immersed vertical barriers, for different values of $G_1 = G_2 = 0.1$; $G_1 = 0.25$, $G_2 = 0.5$; $G_1 = 0.5$, $G_2 = 0.25$; $G_1 = 0.5 + 0.5i$, $G_2 = 0.75 + 0.5i$ and a fixed value of $\theta = 45°$, $\frac{b}{a} = 1.3$, and $\frac{l}{a} = 1$

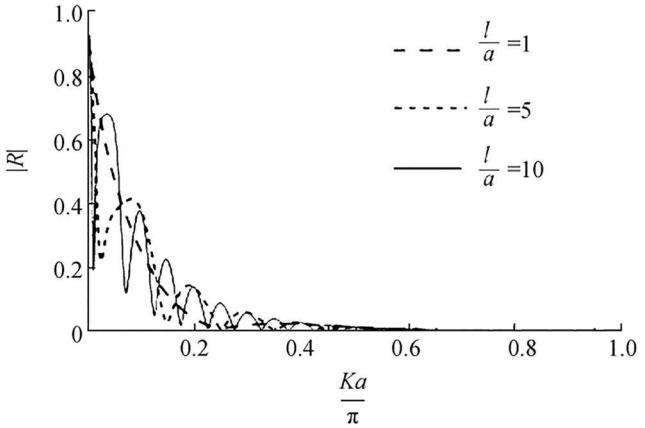

Fig. 28 Reflection coefficients for two submerged barriers, for different values of $\frac{l}{a} = (1, 5, 10)$ and a fixed value of $\theta = 0°$, $G_1 = G_2 = 1$, and $\frac{b}{a} = 1$

an oblique incident wave. These results for $|R|$ coincide exactly with those presented by Roy et al. (2016). By taking $\frac{b}{a} = 1$ and $\frac{l}{a} \to 0$, the structure reduces to a single partially immersed porous barrier, which was studied by Manam and Sivanesan (2016). The curves of $|R|$ are depicted against the wave number Ka for different values of $G_1 = G_2 = 0$, $G_1 = G_2 = 0.1$, $G_1 = 1 = G_2 = 0.5$, $G_1 = G_2 = 1$, $G_1 = G_2 = 1 + i$, $G_1 = G_2 = 1 + 2i$ in the case of a normal incident wave in Fig. 7. The curves of Fig. 7 are almost the same as those presented by Manam and Sivanesan (2016).

In Fig. 8, the curves of $|R|$ and $|T|$ are plotted for two different values of $\frac{b}{a} (= 1, 1.3)$ and a fixed value of $\theta = 0°$, $G_1 = G_2 = 0$, and $\frac{l}{a} = 5$. For the case of two identical fully submerged barriers ($b/a = 1$), the curves of $|R|$ and $|T|$ in Fig. 8 coincide with the curves in Fig. 3 of Jarvis (1971). For the case of two nonidentical fully submerged barriers ($b/a = 1.3$), the curves of $|R|$ in Fig. 8 coincide with the curves in Fig. 6(b) of Roy et al. (2016). These findings indicate the correctness of the results obtained by the present configuration. With the assumption of $\frac{b}{a} = 1$ and $\frac{l}{a} \to 0$, the structure reduces to a single fully submerged porous barrier, which was studied by Manam and Sivanesan (2016). In the case of a normal incident wave, the curves of $|R|$ are depicted against the wave number Ka for different values of $G_1 = G_2 = 0$, $G_1 = G_2 = 0.1$, $G_1 = G_2 = 0.5$ in Fig. 9. The curves of Fig. 9 coincide exactly with those presented by Manam and Sivanesan (2016).

6.2 For Partially Immersed Barriers

In Figs. 10 and 11, the curves of $|R|$ are plotted against the wave number for equal and different porosity, respectively, for a fixed value of $\frac{l}{a} = 1$ *and* $\theta = 0°$ and for different values of length ($\frac{b}{a} = 1, 1.1, 1.2$). The value of $|R|$ is larger for unequal barriers than for equal barriers. Also, for small (<0.1) and large (>0.9) wave numbers, the reflection coefficients are the same for equal and unequal barriers. A comparison

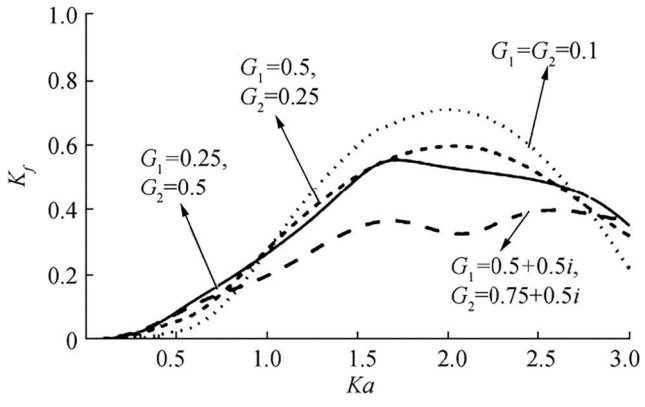

Fig. 27 Wave force for two partially immersed vertical barriers, for different values of $G_1 = G_2 = 0.1$; $G_1 = 0.25$, $G_2 = 0.5$; $G_1 = 0.5$, $G_2 = 0.25$; $G_1 = 0.5 + 0.5i$, $G_2 = 0.75 + 0.5i$ and a fixed value of $\theta = 0°$, $\frac{b}{a} = 1.3$, and $\frac{l}{a} = 1$

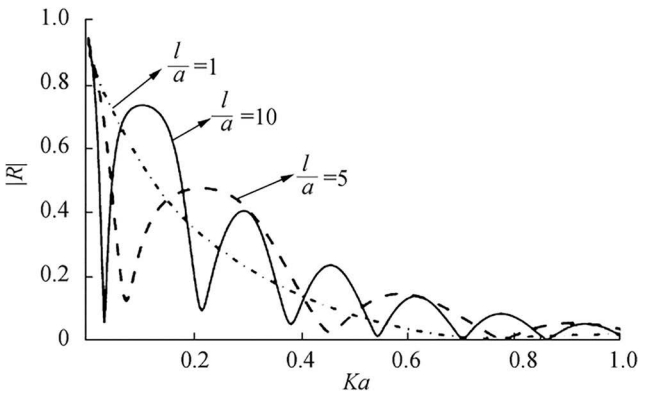

Fig. 29 Reflection coefficient for two submerged vertical barriers, for different values of $\frac{l}{a} (= 1, 5, 10)$ and a fixed value $G_1 = G_2 = 1$, $\frac{b}{a} = 1.3$, and $\theta = 0°$

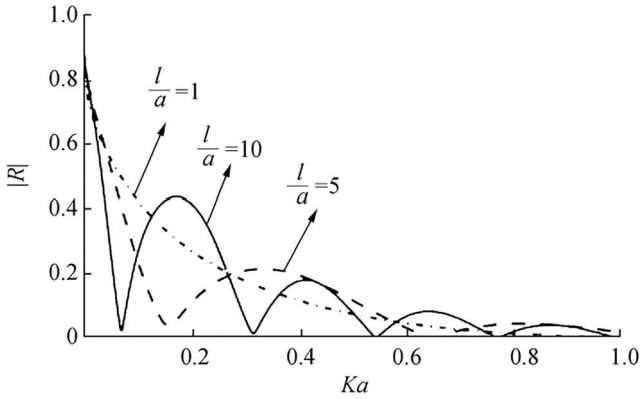

Fig. 30 Reflection coefficient for two submerged vertical barriers, for different values of $\frac{l}{a}(=1,5,10)$ and a fixed value of $G_1 = G_2 = 1$, $\frac{b}{a} = 1.3$, and $\theta = 45°$

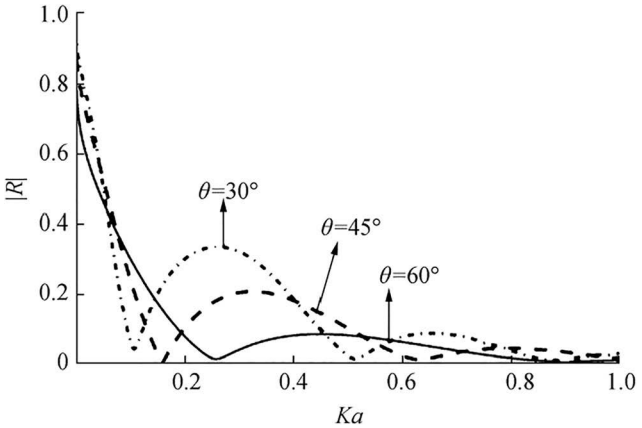

Fig. 32 Reflection coefficient for two submerged vertical barriers, for different values of $\theta(=30°, 45°, 60°)$ and a fixed value of $G_1 = 1$, $G_2 = 1 + 0.5i$, $\frac{b}{a} = 1.3$, and $\frac{l}{a} = 5$

between these two figures shows that $|R|$ is less when the porosity is different for two barriers.

The effect of distance between two barriers on $|R|$ is shown in Figs. 12, 13, 14, and 15, respectively. In Figs. 12 and 13, the graphs are plotted for three different values of $l/a(=1, 2, 3)$ and for a fixed value of $\theta = 0°$ and $b/a = 1$ with equal and different porosity. In Figs. 14 and 15, the graphs are depicted for three different values of $l/a(=1, 2, 3)$ and for a fixed value of $\theta = 0°$ and $b/a = 1.2$ with different porosity. These figures clearly show that for a small wave number, the values of $|R|$ increase and shift toward the right as the distance decreases. By contrast, for a large wave number, the values of $|R|$ increase and shift toward the right as the distance increases. From Figs. 13 and 14, we can conclude that the zeros of $|R|$ are abolished for nonidentical barriers unlike for identical barriers. Moreover, the peak value of $|R|$ decreases as the porosity increases for equal and unequal barriers.

The influence of angle of incidence on $|R|$ for two nonidentical permeable barriers with different porosity is investigated in Figs. 16, 17, 18, and 19. These graphs are plotted for three different values of $\theta(=30°, 45°, 60°)$ and for a fixed value of $b/a = 1.2$ and $l/a = 3$ with different porosity for two barriers. The peak value of $|R|$ decreases as the angle of incidence increases. A comparison between Figs. 16 and 17 shows that the maximum values of $|R|$ reduce due to the inertial effect on porous barriers. A comparison between Figs. 18 and 19 shows a considerable increase in the minimum values of $|R|$ and a decrease in the oscillation of the reflection curves. From all these figures, we can conclude that the value of $|R|$ is small when the porosity is large. In the case of a high value of porosity for a larger barrier, the zeros of $|R|$ exist.

The effect of porosity on $|R|$ for two unequal barriers with oblique and normal incidence is investigated in Figs. 20 and 21, respectively. These graphs are plotted for five different values of $G_1 = G_2 = 0$; $G_1 = G_2 = 0.5$; $G_1 = 1$, $G_2 = 0.75$; $G_1 = 0.75$, $G_2 = 1$; $G_1 = 1 + 0.5i$, $G_2 = 1.25$ and a fixed value of $\frac{b}{a} = 1.2$ and $\frac{l}{a} = 3$ for oblique and normal incident waves. These figures show that the minimum and maximum values of $|R|$ are obtained at the specific values of wave numbers corresponding to all values of porous effect parameters. However, the value of $|R|$ decreases as the value of porous

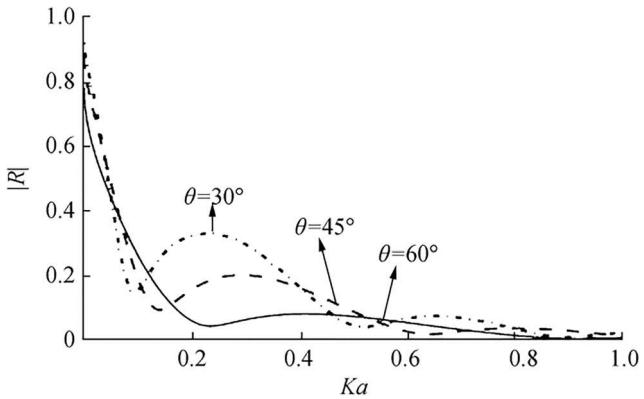

Fig. 31 Reflection coefficient for two submerged vertical barriers, for different values of $\theta(=30°, 45°, 60°)$ and a fixed value of $G_1 = 2$, $G_2 = 1$, $\frac{b}{a} = 1.3$, and $\frac{l}{a} = 5$

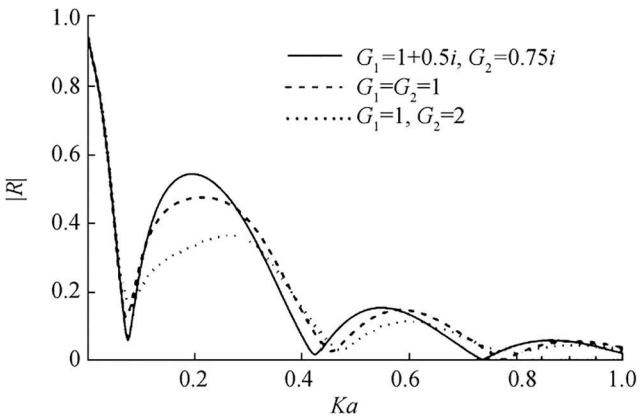

Fig. 33 Reflection coefficient for two submerged vertical barriers, for different values of $G_1 = G_2 = 1$; $G_1 = 1$, $G_2 = 2$; $G_1 = 1 + 0.5i$, $G_2 = 0.75i$ and a fixed value of $\theta = 0°$, $\frac{b}{a} = 1.3$, and $\frac{l}{a} = 5$

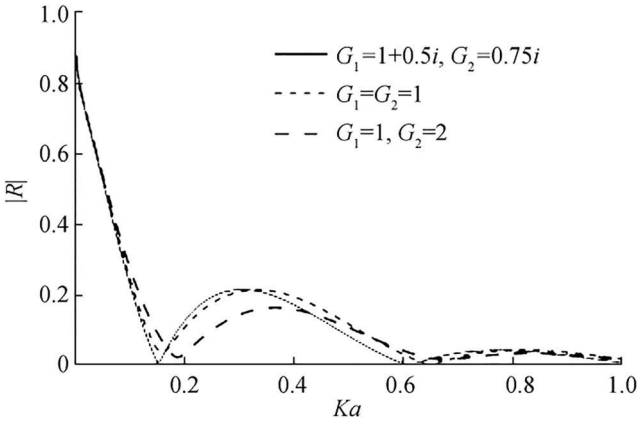

Fig. 34 Reflection coefficient for two submerged vertical barriers, for different values of $G_1 = G_2 = 1$; $G_1 = 1$, $G_2 = 2$; $G_1 = 1 + 0.5i$, $G_2 = 0.75i$ and a fixed value of $\theta = 45°$, $\frac{b}{a} = 1.3$, and $\frac{l}{a} = 5$

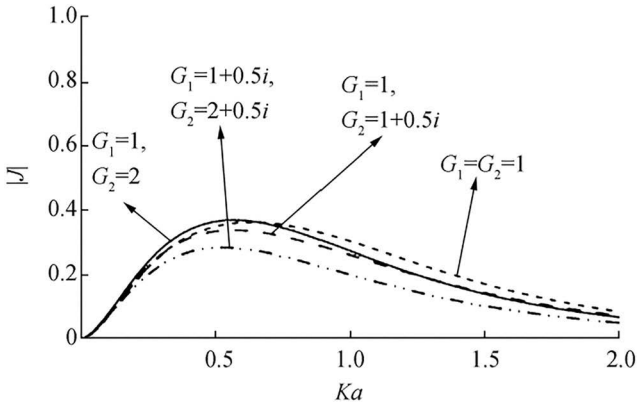

Fig. 36 Dissipated energy for two submerged vertical barriers, for different values of $G_1 = G_2 = 1$; $G_1 = 1$, $G_2 = 2$; $G_1 = 2$, $G_2 = 1$; $G_1 = 1$, $G_2 = 1 + 0.5i$; $G_1 = 1 + 0.5i$, $G_2 = 2 + 0.5i$ and a fixed value of $\theta = 0°$, $\frac{b}{a} = 1.3$, and $\frac{l}{a} = 1$

effect parameters increases. When we take a small value of porosity for the smaller barrier, then the value of $|R|$ is less than that for greater porosity for a large barrier.

The amount of dissipated energy for two equal or unequal barriers is plotted against the wave number in Figs. 22, 23, and 24. In Figs. 22 and 23, the graphs are plotted for five different values of $G_1 = G_2 = 1$; $G_1 = 1$, $G_2 = 2$; $G_1 = 2$, $G_2 = 1$; $G_1 = 1$, $G_2 = 1 + 0.5i$; $G_1 = 1 + 0.5i$, $G_2 = 2 + 0.5i$ and a fixed value of $\theta = 45°$ and $\frac{l}{a} = 1$ for equal and unequal barriers. The graph in Fig. 24 is plotted for four different values of $G_1 = G_2 = 1$; $G_1 = 1$, $G_2 = 2$; $G_1 = 1$, $G_2 = 1 + 0.5i$; $G_1 = 1 + 0.5i$, $G_2 = 2 + 0.5i$ and a fixed value of $\theta = 0°$, $\frac{l}{a} = 1$, and $\frac{b}{a} = 1.3$. For a small wave number $Ka < 0.2$, energy dissipation decreases as the porosity increases. However, for large wave numbers, a large amount of energy is dissipated as the porosity decreases. Moreover, the curve of energy dissipation for normal incidence is more oscillatory than that for oblique incidence.

The coefficient of wave force for two equal or unequal barriers is plotted against the wave number in Figs. 25, 26, and 27. The graphs in Figs. 25 and 26 are plotted for four different values of $G_1 = G_2 = 0.1$; $G_1 = 0.25$, $G_2 = 0.5$; $G_1 = 0.5$, $G_2 = 0.25$; $G_1 = 0.5 + 0.5i$, $G_2 = 0.75 + 0.5i$ and a fixed value of $\theta = 45°$ and $\frac{l}{a} = 1$ for equal and unequal barriers. The graph in Fig. 27 is plotted for four different values of $G_1 = G_2 = 0.1$; $G_1 = 0.25$, $G_2 = 0.5$; $G_1 = 0.5$, $G_2 = 0.25$; $G_1 = 0.5 + 0.5i$, $G_2 = 0.75 + 0.5i$ and a fixed value $\theta = 0^0$, $\frac{l}{a} = 1$, and $\frac{b}{a} = 1.3$. For a small wave number $Ka < 1$, the coefficient of wave force decreases as the porosity increases. However, for large wave numbers, the coefficient of wave force increases as the porosity decreases. Moreover, the curves of complex porosity are more oscillatory than the curves of real porosity due to inertial effect.

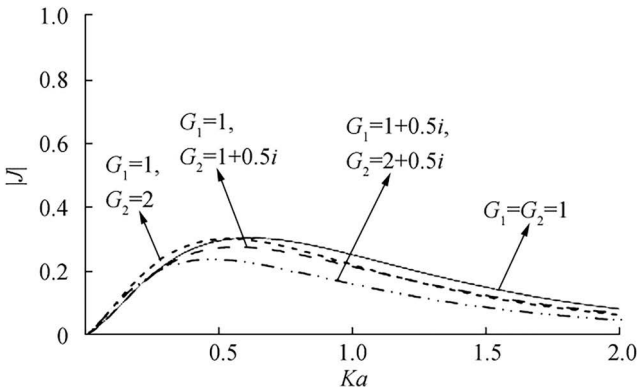

Fig. 35 Dissipated energy for two submerged vertical barriers, for different values of $G_1 = G_2 = 1$; $G_1 = 1$, $G_2 = 2$; $G_1 = 1$, $G_2 = 1 + 0.5i$; $G_1 = 1 + 0.5i$, $G_2 = 2 + 0.5i$ and a fixed value of $\theta = 30°$, $\frac{b}{a} = 1$, and $\frac{l}{a} = 1$

6.3 For Submerged Barriers

We present the numerical result for two fully submerged equal and unequal barriers. The effect of distance between the two barriers on $|R|$ is shown in Figs. 28, 29, and 30. In Fig. 28, the graphs are plotted against $\frac{Ka}{\pi}$ for three different values of l/a(=1, 5, 10) and for a fixed value of $\theta = 0^o$, $b/a = 1$, and $G_1 =$

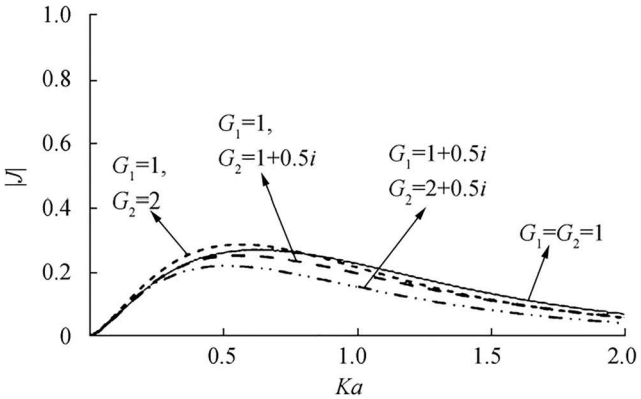

Fig. 37 Dissipated energy for two submerged vertical barriers, for different values of $G_1 = G_2 = 1$; $G_1 = 1$, $G_2 = 2$; $G_1 = 2$, $G_2 = 1$; $G_1 = 1$, $G_2 = 1 + 0.5i$; $G_1 = 1 + 0.5i$, $G_2 = 2 + 0.5i$ and a fixed value of $\theta = 30°$, $\frac{b}{a} = 1.3$, and $\frac{l}{a} = 1$

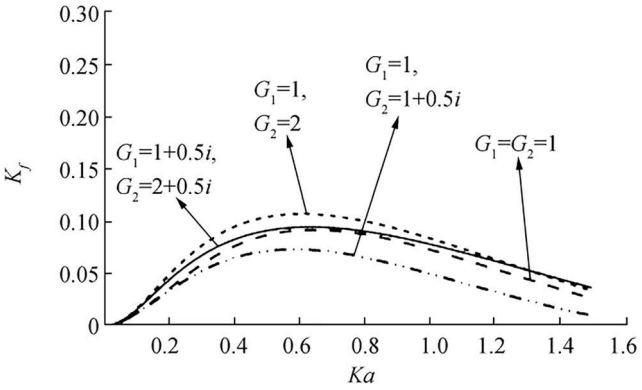

Fig. 38 Wave force for two submerged vertical barriers, for different values of $G_1 = G_2 = 1$; $G_1 = 1$, $G_2 = 2$; $G_1 = 1$, $G_2 = 1 + 0.5i$; $G_1 = 1 + 0.5i$, $G_2 = 2 + 0.5i$ and a fixed value of $\theta = 30°$, $\frac{b}{a} = 1$, and $\frac{l}{a} = 1$

$G_2 = 1$. In Figs. 29 and 30, the graphs are plotted against Ka for three different values of l/a(=1, 5, 10) and for a fixed value of $b/a = 1.3$ and $G_1 = G_2 = 1$ for normal and oblique incidence, respectively. These figures, clearly show that for a small wave number, the values of $|R|$ are high. However, for a large wave number, the values of $|R|$ become almost zero. The minimum values of $|R|$ are shifted shift toward the right as the distance decreases.

The influence of angle of incidence on $|R|$ for two unequal permeable barriers with different porosity is shown in Figs. 31 and 32. These graphs are plotted for three different values of θ(=30°, 45°, 60°) and for a fixed value of $b/a = 1.3$ and $l/a = 5$ with different porosity for two barriers. The peak value of $|R|$ decreases as the angle of incidence increases. From these figures, we can conclude that the value of $|R|$ is small when the porosity is large. In the case of a high value of porosity for a smaller barrier, the zeros of $|R|$ exist.

The effect of porosity on $|R|$ for two unequal barriers is shown in Figs. 33 and 34 for normal and oblique incident wave, respectively. These graphs are plotted for three different values of $G_1 = G_2 = 1$; $G_1 = 1$, $G_2 = 2$; $G_1 = 1 + 0.5i$, $G_2 = 0.75i$ and a fixed value of $\frac{b}{a} = 1.3$ and $\frac{l}{a} = 5$ for normal and

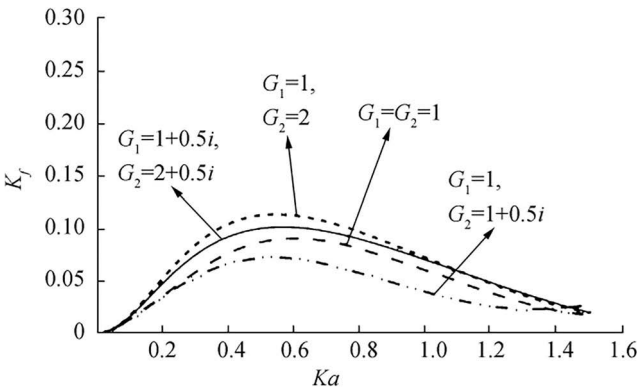

Fig. 39 Wave force for two submerged vertical barriers, for different values of $G_1 = G_2 = 1$; $G_1 = 1$, $G_2 = 2$; $G_1 = 1$, $G_2 = 1 + 0.5i$; $G_1 = 1 + 0.5i$, $G_2 = 2 + 0.5i$ and a fixed value of $\theta = 0°$, $\frac{b}{a} = 1.3$, and $\frac{l}{a} = 1$

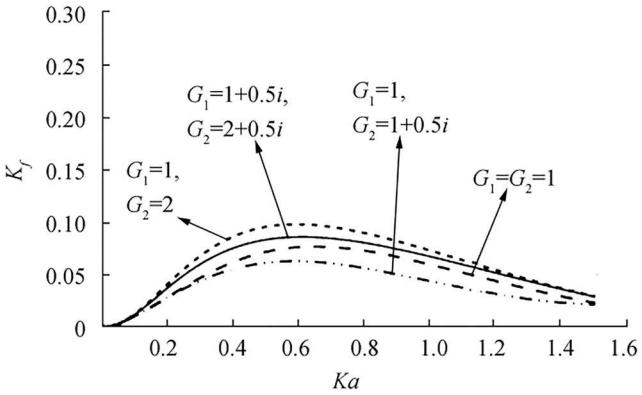

Fig. 40 Wave force for two submerged vertical barriers, for different values of $G_1 = G_2 = 1$; $G_1 = 1$, $G_2 = 2$; $G_1 = 1$, $G_2 = 1 + 0.5i$; $G_1 = 1 + 0.5i$, $G_2 = 2 + 0.5i$ and a fixed value $\theta = 30°$, $\frac{b}{a} = 1.3$, and $\frac{l}{a} = 1$

oblique incident waves. These figures show that the peak values of $|R|$ are obtained for specific values of wave numbers for all different porosity. However, the value of $|R|$ decreases as the value of porous effect parameters increases. Moreover, for the oblique incident wave, the number of oscillations of the curves of $|R|$ is less than that of the normal incident wave.

The amount of dissipated energy for two equal or unequal barriers is plotted against the wave number in Figs. 35, 36, and 37. In Figs. 35 and 37, the graphs are plotted for four different values of $G_1 = G_2 = 1$; $G_1 = 1$, $G_2 = 2$; $G_1 = 1$, $G_2 = 1 + 0.5i$; $G_1 = 1 + 0.5i$, $G_2 = 2 + 0.5i$ and a fixed value of $\theta = 30°$ and $\frac{l}{a} = 1$ for equal and unequal barriers. The graph in Fig. 36 is plotted for four different values of $G_1 = G_2 = 1$; $G_1 = 1$, $G_2 = 2$; $G_1 = 1$, $G_2 = 1 + 0.5i$; $G_1 = 1 + 0.5i$, $G_2 = 2 + 0.5i$ and a fixed value of $\theta = 0^o$, $\frac{l}{a} = 1$, and $\frac{b}{a} = 1.3$. For a small wave number $Ka < 0.3$, the energy dissipation decreases as the porosity increases. However, for large wave numbers, a large amount of energy is dissipated as the porosity decreases. Moreover, the value of energy dissipation for normal incidence is more than that for oblique incidence.

The coefficient of wave force for two equal or unequal barriers is plotted against the wave number in Figs. 38, 39, and 40. The graphs in Figs. 38 and 40 are plotted for four different values of $G_1 = G_2 = 1$; $G_1 = 1$, $G_2 = 2$; $G_1 = 1$, $G_2 = 1 + 0.5i$; $G_1 = 1 + 0.5i$, $G_2 = 2 + 0.5i$ and a fixed value of $\theta = 30°$ and $\frac{l}{a} = 1$ for equal and unequal barriers. The graph in Fig. 39 is plotted for four different values of $G_1 = G_2 = 1$; $G_1 = 1$, $G_2 = 2$; $G_1 = 1$, $G_2 = 1 + 0.5i$; $G_1 = 1 + 0.5i$, $G_2 = 2 + 0.5i$ and a fixed value of $\theta = 0$, $\frac{l}{a} = 1$, and $\frac{b}{a} = 1.3$. The peak value of the coefficient of wave force decreases as the porosity decreases. Moreover, the value of the coefficient of wave force for complex porosity is less than that for real porosity.

7 Conclusion

This study investigates the scattering of oblique incident waves by two partially immersed and two totally submerged unequal barriers with different porosity. With the use of Havelock's expansion of wave potential and the condition on the permeable barriers, the problem is transformed into two integral equations, which are then approximated by employing single-term Galerkin approximation method. Accurate values of reflection and transmission coefficients are obtained for both the problems. An energy identity equation is derived using Green's integral theorem, which states that some energy is dissipated due to the effect of porosity on barriers. The coefficient of wave force is also derived. The numerical results of hydrodynamics quantities are illustrated graphically. The derived result coincides analytically and graphically with the results that have already been presented in the literature. This comparison proves the rapid convergence of our method in contrast to the method available in the literature. We discuss the results for two equal barriers and two unequal barriers. The computational result clearly shows that for some fixed wave numbers, the peak value of reflection coefficient decreases when the value of porosity increases for oblique and normal incident waves. In the presence of porosity, the length and distance between barriers play an important role in the scattering behavior of the surface waves by two partially immersed and two submerged barriers. Also, the computed results of reflection and transmission coefficients satisfy the energy identity for permeable and impermeable barriers. An infinite number of wave periods exist at which waves are fully transmitted with the effect of porosity. As a result of porosity, for a small wave number, the reflection is negligible for the case of partially immersed barriers, but the transmission is negligible for two submerged barriers.

This study can be further extended to investigate the problems of water wave scattering by multiple thin vertical porous barriers in uniform finite depth water or infinite deep water. The Galerkin approximation involving simple polynomials as basis can be used to obtain the solution of integral equations arising in the problems of thin vertical multiple porous barriers.

Funding This work is partially supported by a SERB, DST(EMR/2016/005315).

References

Banerjea S, Kanoria M, Dolai DP, Mandal BN (1996) Oblique wave scattering by a submerged thin wall with gap in finite depth water. Appl Ocean Res 18:319–327. https://doi.org/10.1016/S0141-1187(97)00002-3

Behera H, Sahoo T (2014) Gravity wave interaction with porous structures in two-layer fluid. J Eng Math 87(1):73–97. https://doi.org/10.1007/s10665-013-9667-0

Bhattacharjee J, Guedes Soares C, (2011) Vertical porous membrane barrier for coastal structure near a wall, Coastal and Maritime Mediterranean Conference, Edition 2, Tanger, Maroc, 15–20. DOI: https://doi.org/10.5150/cmcm.2011.004

Chwang AT (1983) A porous wave maker theory. J Fluid Mech 132:395–406. https://doi.org/10.1017/S0022112083001676

Das S, Bora SN (2018) Oblique water wave damping by two submerged thin vertical porous plates of different heights. Comput Appl Math 37(3):3759–3779. https://doi.org/10.1007/s40314-017-0545-7

Das P, Dolai DP, Mandal BN (1997) Oblique wave diffraction by parallel thin vertical barriers with gaps. J Waterw Port Coast Ocean Eng 123:163–171. https://doi.org/10.1061/(ASCE)0733-950X(1997)123:4(163)

De S, Mandal BN, Chakrabarti A (2010) Use of abel integral equations in water wave scattering by two surface piercing barriers. Wave Motion 47:279–288. https://doi.org/10.1016/j.wavemoti.2009.12.002

Dean WR (1945) On the reflection of surface waves by a flat plate floating vertically. Math Proc Camb Philos Soc 41:231–238

Evans DV (1970) Diffraction of water waves by a submerged vertical plate. J Fluid Mech 40:433–451. https://doi.org/10.1017/S0022112070000253

Evans DV, Morris CAN (1972) Complementary approximations to the solution of a problem in water waves. J Inst Math Applications 10(1):1–9. https://doi.org/10.1093/imamat/10.1.1

Gayen R, Mondal A (2014) A hypersingular integral equation approach to the porous plate problem. Appl Ocean Res 46:70–78. https://doi.org/10.1016/j.apor.2014.01.006

Isaacson M, Premasiri S, Yang G (1998) Wave interactions with vertical slotted barriers, J. Waterw Port Coast Ocean Eng 124:118–126. https://doi.org/10.1061/(ASCE)0733-950X(1998)124:3(118)

Isaacson M, Baldwin J, Premasiri S, Yang G (1999) Wave interactions with double slotted barriers. Appl Ocean Res 21:81–91. https://doi.org/10.1016/S0141-1187(98)00039-X

Jarvis RJ (1971) The scattering of surface waves by two vertical plane barriers. J Inst Maths Applic 7:207–215

Kanoria M, Mandal BN (1996) Oblique wave diffraction by two parallel vertical barriers with submerged gaps in water of uniform finite depth. J Tech Phys 37:187–204

Karmakar D, Guedes Soares C (2014) Wave transmission due to multiple bottom-standing porous barriers. Ocean Eng 80:50–63. https://doi.org/10.1016/j.oceaneng.2014.01.012

Karp NS, Karal CF (1962) The elastic field behaviour in the neighbourhood of a crack of arbitrary angle. Commun Pure Appl Math 15:413–421. https://doi.org/10.1002/cpa.3160150404

Lee MM, Chwang AT (2000) Scattering and radiation of water waves by permeable barriers. Phys Fluids 12:54–65. https://doi.org/10.1063/1.870284

Levine H, Rodemich E, 1969. Scattering of surface waves on an ideal fluid, Tech rep, DTIC Document

Li AJ, Liu Y, Li HJ (2015) Accurate solutions to water wave scattering by vertical thin porous barriers. Math Probl Eng 2015:1–11. https://doi.org/10.1155/2015/985731

Macaskill C (1979) Reflection of water waves by a permeable barrier. J Fluid Mech 75:141–157. https://doi.org/10.1017/S0022112079001385

Manam SR, Sivanesan M (2016) Scattering of water waves by vertical porous barriers: an analytical approach. Wave Motion 67:89–101. https://doi.org/10.1016/j.wavemoti.2016.07.008

Mandal BN, Chakrabarti A (2000) Water wave scattering by barriers. WIT Press, Southampton, pp 24–25

McIver P (1985) Scattering of surface waves by two surface piercing vertical barriers. IMA J Appl Math 35(1):1–17. https://doi.org/10.1093/imamat/35.3.339

Mohapatra SC, Sahoo T, Guedes Soares C (2018) Surface gravity wave interaction with a submerged horizontal flexible porous plate. Appl Ocean Res 78:61–74. https://doi.org/10.1016/j.apor.2018.06.002

Newman JN (1974) Interaction of water waves with two closely spaced vertical obstacles. J Fluid Mech 66:97–106. https://doi.org/10.1017/S0022112074000085

Porter R, Evans DV (1995) Complementary approximations to wave scattering by vertical barriers. J Fluid Mech 294:155–180. https://doi.org/10.1017/S0022112095002849

Roy R, Basu U, Mandal BN (2016) Oblique water scattering by two unequal vertical barriers. J Eng Math 97:119–133. https://doi.org/10.1007/s10665-015-9800-3

Sollitt CK, Cross RH (1972) Wave transmission through permeable breakwaters. Coast Eng Proc 1:1827–1846. https://doi.org/10.1061/9780872620490.106

Ursell F (1947) The effect of a fixed vertical barrier on surface waves in deep water. Math Proc Camb Philos Soc 43:374–382. https://doi.org/10.1017/S0305004100023604

Yu X (1995) Diffraction of water waves by porous breakwaters, J. Waterw Port Coast Ocean Eng 121:275–282. https://doi.org/10.1061/(ASCE)0733-950X(1995)121:6(275)